Circular Economy 2 (2023) 100064

Contents lists available at ScienceDirect

Circular Economy

journal homepage: www.journals.elsevier.com/circular-economy

Original Research

Synthesis and electrochemical properties of porous carbon materials from sludge sources

Muqian Guo, Ying Li*, Pengxiao Liu, Xiaotian Jia, Xingnan Zhang

School of Environmental and Safety Engineering, North University of China, Taiyuan 030051, China

ARTICLE INFO

Article history:
Received 19 October 2023
Received in revised form
17 November 2023
Accepted 19 November 2023
Available online 21 November 2023

Keywords:
Sludge
Humic acid (HA)
Electrode materials
Electrochemical performance

ABSTRACT

Anaerobic digestion sludge technology is a green and efficient method of treating sludge. However, the presence of humic acid (HA) in sludge can inhibit methanogenic efficiency, and it is necessary to reduce its impact on biogas production by removal or pretreatment. HA, a graphene oxide material can be used to produce high-performance energy-storage materials. Thus, this study examined the sludge source of HA as a precursor, and different electrode materials were prepared by varying the reaction conditions. The structure and electrochemical properties of the electrode materials were analyzed. The results showed that the electrode material prepared using KOH as an activator at 700 °C exhibited optimal performance, with a high specific surface area (1480.53 $m^2 \cdot g^{-1}$), pore volume (0.943 $cm^3 \cdot g^{-1}$), specific capacitance (185.9 $F \cdot g^{-1}$), and equivalent series resistance (0.73 Ω). The material maintained 97.8% of its specific capacitance after 1000 cycles at a current density of 1 $A \cdot g^{-1}$ with benign cycle stability. This study confirmed that the production of HA as an electrode material at a low cost with good performance presents significant prospects.

© 2023 The Author(s). Published by Elsevier B.V. on behalf of Tsinghua University Press. This is an open access article under the CC BY-NC-ND license (http://creativecommons.org/licenses/by-nc-nd/4.0/).

1. Introduction

With rapid economic development and the continuous improvement of living standards, the use of water resources has significantly increased. According to the Ministry of Housing and Urban–Rural Development of China, as of the end of 2021, the annual sewage discharge in China was 62507.63 million cubic meters, with 2827 sewage treatment plants and an annual dry sludge production of 14.23 million tons.

Anaerobic digestion technology can simultaneously stabilize easily biodegradable organic matter, reduce pathogenic microorganisms, reduce sludge volume, and recover biomass energy. This technology is the predominant approach to sludge stabilization treatment in domestic and international contexts (Dai et al., 2021). In the European Union, 69% of wastewater treatment plants are equipped with sludge digestion and biogas utilization facilities. Anaerobic digestion is the prevalent treatment method (Li et al., 2013). During the anaerobic digestion process, microorganisms convert organic matter in the sludge into methane, mitigating China's energy shortage through biogas power generation technology. Humic substances are the primary organic constituents of sludge, and researchers have determined that the humic acid (HA) content in sludge comprises 26%–28% of the organic matter in sludge (Tsutsuki et al., 1978). HA adversely influences the hydrogenotrophic methane-producing process by inhibiting the activity of hydrogenotrophic methanogens, thereby reducing the efficiency of methane production (Climent et al., 2007). However, HA contains abundant oxygen functional groups (carboxyl, phenolic, aldehyde, and ketone groups), and HA-based electrode materials exhibit outstanding storage and cycling performance (Zhu et al., 2015.). Thus, the conversion of the HA-rich content in sludge into electrode materials reduces the HA content (indirectly enhancing the methane production efficiency) and generates energy-storage materials.

Yin et al. (2014) first utilized HA as a raw material to synthesize activated carbon (AC) through a high-temperature activation process with KOH. The results indicated that the AC exhibited a high specific surface area (up to 2990.32 $m^2 \cdot g^{-1}$) and maintained 92% of its initial capacitance even after 9000 cycles at a high current density of 1 $A \cdot g^{-1}$. Xing et al. (2017) utilized commercial HA as a raw material to prepare graphene nanosheets through a thermal reduction method. The nanosheets exhibited a high specific surface area (495 $m^2 \cdot g^{-1}$) and pore volume (2.987 $cm^3 \cdot g^{-1}$). At a current density of 50 $mA \cdot g^{-1}$, the nanosheets exhibited a significant

* Corresponding author.
E-mail address: lying@nuc.edu.cn (Y. Li).

https://doi.org/10.1016/j.cec.2023.100064
2773-1677/© 2023 The Author(s). Published by Elsevier B.V. on behalf of Tsinghua University Press. This is an open access article under the CC BY-NC-ND license (http://creativecommons.org/licenses/by-nc-nd/4.0/).

specific capacitance (272 $F \cdot g^{-1}$) and maintained a capacitance retention rate exceeding 96.5% after 8000 cycles, indicating excellent electrochemical performance (Xing et al., 2017). Microporous and mesoporous structures were observed in the resulting samples of HA extracted from brown coal, with a high specific surface area of 1730 $m^2 \cdot g^{-1}$ (Siemieniewska et al., 1991). Coal-derived HA was utilized as a raw material to prepare hierarchical porous carbons (HPCs) through the KOH activation method (Huang, Kang, et al., 2016). The results showed that the HPCs exhibited a hierarchical porous structure (micropores, mesopores, and macropores). The HPC-based electrodes exhibited a substantial capacitance of 201 $F \cdot cm^{-3}$ at a current density of 5 $A \cdot g^{-1}$. Thus, it can be inferred that sludge-derived HAs possess inherent properties suitable for the preparation of porous electrode materials.

Thus, this study investigated dehydrated sludge (Jia et al., 2022; Li et al., 2023). Under the premise of the "alkali pretreatment of sludge," according to the acid–base theory and the classification criteria of activators in the activation mechanism (Chen et al., 2013), different HA-based energy-storage materials (HAC) were prepared using acids (H_3PO_4), salts ($ZnCl_2$), and alkalis (KOH) as activators. After the activators were determined, various HACs were synthesized by varying the activation temperature. Thereafter, the electrochemical performance of the HAC materials was investigated to examine the effects of the activator and activation temperature.

2. Experimental materials and methods

2.1. Materials

Sludge was obtained from a large sewage treatment plant in Taiyuan City, Shanxi Province, China. Excess sludge was obtained after concentration and dehydration processes. The sludge was naturally air-dried, crushed, ground to a size below 20 meshes, and stored at 20 °C. All the chemicals used were of analytical grade.

A water-bath constant-temperature oscillator (WE-2, Tianjin Ounuo Instrument and Meter Co., Ltd.) was used in the sludge alkali-treatment process. The calcination equipment used for preparing biomass charcoal was a tube furnace (SK-G08123K-5–875, Tianjin Zhonghuan Electric Furnace Co., Ltd.).

Regarding physicochemical properties, the structural analysis of the electrode materials was conducted using a field-emission scanning electron microscope (ZEISS Gemini 300), a fully automatic surface area and porosity analyzer (Autosorb-IQ), an X-ray diffractometer (Empyrean), and a confocal micro Raman spectrometer (LabRAM HR Evolution).

For electrochemical testing, cyclic voltammetry (CV) and electrochemical impedance spectroscopy (EIS) were conducted using an electrochemical workstation (CHI660E). Constant current galvanostatic charge–discharge (GCD) and cyclic performance tests were conducted using a blue electric testing system (CT2001A).

2.2. Material preparation

2.2.1. Alkaline pretreatment of sludge

The air-dried sludge sample (6 g) was mixed with a 0.2 $mol \cdot L^{-1}$ NaOH solution at a solid-liquid ratio of 1:50 and subjected to constant-temperature agitation for 24 h. The mixture was subsequently centrifuged at 6000 $r \cdot min^{-1}$ for 10 min. The supernatant was poured into a 1-L beaker and acidified several times with HCL until pH = 1. Thereafter, the solution was left to stand and precipitate for 12 h. The coagulated precipitate was washed to neutrality and centrifuged, and the resulting deposit was freeze-dried to obtain the HA sample.

2.2.2. Preparation of porous carbon materials

(1) The activators (H_3PO_4, $ZnC1_2$, and KOH) were separately dissolved in ultrapure water at a 1:1 ratio, and the mixtures were stirred by magnetic agitation. After drying at 80 °C and grinding using an 80-mesh sieve, the mixtures were placed in a tube furnace and heated to 700 °C under a continuous flow of N_2 gas at a heating rate of 5 $°C \cdot min^{-1}$. The resulting ash was washed with HCl for activation and then rinsed with water until a neutral pH was achieved. Finally, the material was dried in an oven at 80 °C. According to the activator used, the materials were named HAC-P-700, HAC-Zn-700, and HAC-K-700.

(2) The activator determined to be optimal (KOH) was dissolved in ultrapure water at a mass ratio of 1:1 with HA, and the mixture was thoroughly stirred. After drying and grinding, the mixture was carbonized in a tube furnace at 700 °C, 800 °C, and 900 °C for 1 h each. After acid washing, water rinsing, and drying, the resulting materials were named HAC-K-700, HAC-K-800, and HAC-K-900.

2.2.3. Preparation of electrode materials

The HAC electrode material, acetylene black (conductive agent), and polytetrafluoroethylene (binder; 10 wt%) were weighed at a mass ratio of 8:1:1. Thereafter, they were mixed in ethanol until a paste was formed. A small amount of the paste was uniformly coated onto foam nickel substrates with an area of 1×1 cm^2, ensuring that each substrate contained 4.8–5.2 mg of the HA-based material. The coated substrates were dried at 80 °C to obtain working electrodes. A 6 $mol \cdot L^{-1}$ KOH solution was used as the electrolyte. An Hg/HgO electrode and Pt foil electrode were employed as the reference and counter electrodes, respectively, and a three-electrode system was constructed with the prepared working electrode.

3. Results and analysis

3.1. Organic element analysis

An organic element analyzer was used to measure the C, H, N, and O contents in the HA of the sludge source (Table 1). A comparison of HA from different sources revealed that the N content in the sludge-derived HA was 10.08%, which was 8.4 times higher than that of weathered coal-derived HA and significantly higher than those in other HA sources. The carbon material skeleton contains a specific amount of N atoms, which can provide free electrons for the conduction band, thereby enhancing the electrical conductivity of the material (Zhang et al., 2015). The C/N ratio of the sludge-derived HA was 5.21. A lower C/N ratio indicates a higher degree of humification of the sludge-derived organic matter, reflecting higher stability.

3.2. Structural analysis of electrode material

3.2.1. Scanning electron microscopy

The dried HAC materials were uniformly ground in a mortar and sieved to obtain homogeneous materials, which were subjected to

Table 1
Analysis of the humic acid (HA) elements from different sources.

HA	C (%)	H (%)	N (%)	O (%)	C/N
Sludge HA	52.43	6.33	10.08	21.49	5.21
Weathered coal HA	51.2	3.7	1.2	31.3	4.95
Peat HA	50.4	4.95	2.8	39.1	18.00
Straw HA	55.49	8.32	7.01	29.73	7.92

field-emission scanning electron microscopy (FE-SEM) at 700 °C. Fig. 1 shows the SEM images at magnifications of 5 μm and 500 nm. The HAC-P-700 surface was irregular and rough, with practically no observable pore structures, indicating the weak pore-forming effect of H_3PO_4. HAC-Zn-700 and HAC-K-700 exhibited partially scattered pore structures on their surfaces. However, HAC-Zn-700 featured solid granules and uneven pores, indicating a relatively weak activation effect and incomplete pore formation (Zhang et al., 2017). For HAC-K-700, densely arranged honeycomb-like pores were prominent, indicating that KOH was crucial in the carbonization process. Owing to the KOH, the material surface was etched and numerous pore structures were generated. Interconnected porous structures facilitated rapid ion transport and diffusion across the channels, thereby enhancing the electrochemical performance of the material (Cheng et al., 2019).

3.2.2. X-ray diffraction and Raman spectroscopy

Figs. 2(a) and 2(b) show the X-ray diffraction (XRD) patterns of the HAC materials activated by different agents and at varying temperatures. Fig. 2(a) reveals distinct graphite (002) diffraction peaks at approximately $2\theta = 26.5°$ for HAC-K-700 and HAC-Zn-700, indicating their high crystallinities and intact graphite structures.

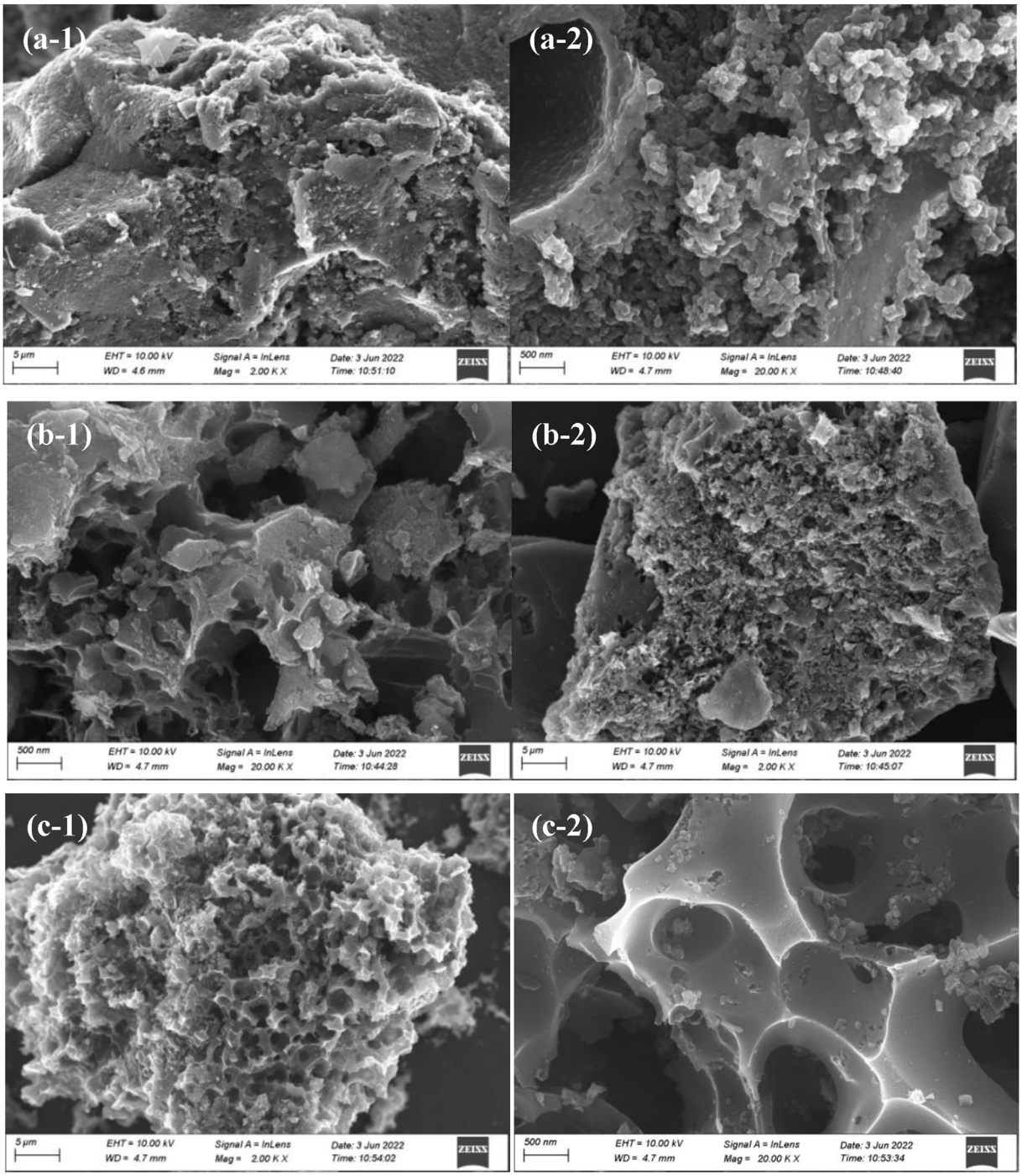

Fig. 1. SEM images of the samples: (a) HAC-P-700, (b) HAC-Zn-700, and (c) HAC-K-700.

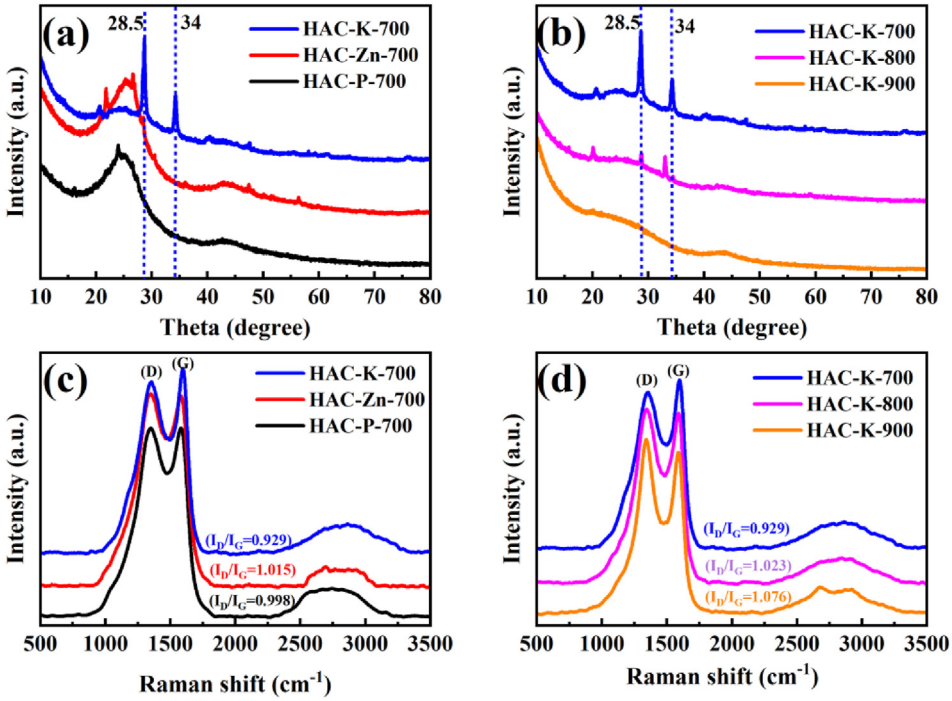

Fig. 2. (a, b) X-ray diffraction (XRD) and (c, d) Raman spectra of each sample.

In addition, observable graphite (004) diffraction peaks at approximately 34° suggested the formation of second-order graphite intercalation compounds (Wei et al., 2022).

HAC-K-700 and HAC-K-800 exhibited sharp diffraction peaks at approximately 28.5° (Fig. 2(b)), indicating the presence of numerous crystalline structures and pronounced order in both materials. The diffraction peaks at approximately 28.5° gradually weakened with an increase in the activation temperature, suggesting a reduction in the microcrystalline graphite structure of the materials. This suggests that the increase in temperature resulted in a relatively strong activation of KOH, leading to excessive etching, which disrupted the microcrystalline graphite structure in both materials. This disruption caused an increase in internal defects and a relatively high degree of disorder. HAC-K-700 exhibited an

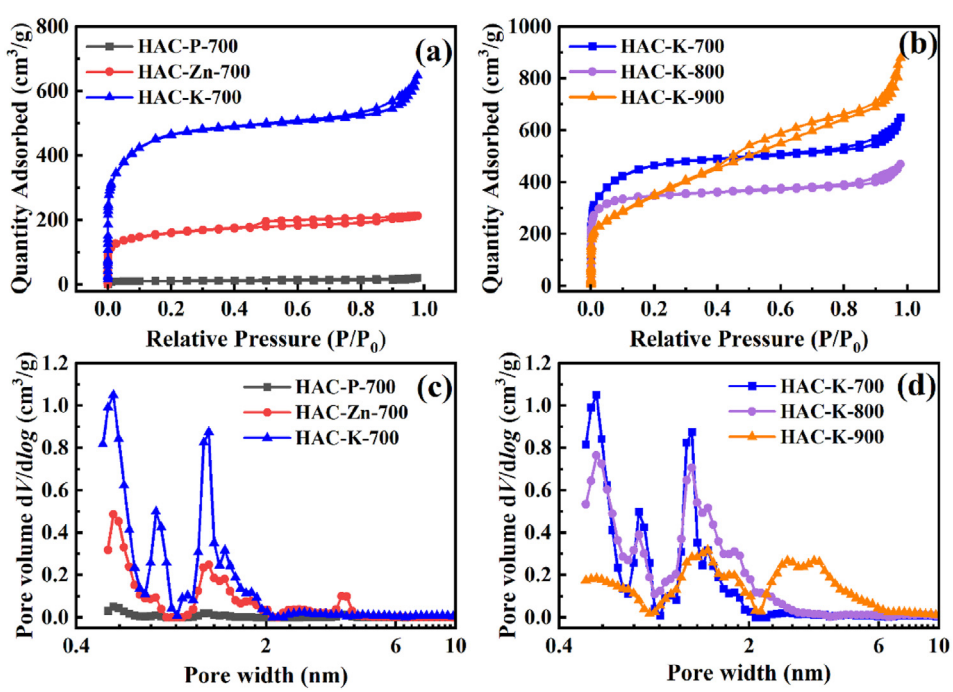

Fig. 3. (a, b) N_2 adsorption-desorption isotherm and (c, d) pore size distribution of the samples.

Table 2
Analysis of specific surface area of electrode materials from different sources.

Sample	S_{BET}[a]/($m^2 \cdot g^{-1}$)	References
Sludge	1480.53	This study
Phenolic resin	1141	Jiang et al. (2014)
Lignite	1024	Li et al. (2016)
Citrus peel	768	Li et al. (2018)
Rice hull	332	Yu et al. (2019)

[a] The specific surface area was determined using the BET method.

evident rightward shift in the overall peak positions, probably because of thermal stress generated during high-temperature calcination.

The degree of graphitization of the HAC materials was further analyzed through Raman spectroscopy (Figs. 2(c) and 2(d)). All the materials exhibited two characteristic peaks, namely the D and G peaks at 1350 and 1580 cm^{-1}, respectively. The D peak was associated with defects and disordered structures in the samples, whereas the G peak represented the orderliness of the graphite structure (Liu et al., 1992). The ratio of the spectral intensities of the D and G peaks is denoted by ID/IG. A high ID/IG ratio indicates a high number of internal defect sites and a significantly disordered arrangement in the material (Zhao et al., 2016). Fig. 2(d) shows that the ID/IG value of the material continuously increased with an increase in the calcination temperature, indicating that excessively high temperatures led to a significantly disordered internal structure and high defect disorder. Figs. 2(c) and 2(d) show that the ID/IG value of HAC-K-700 was the lowest at 0.929, suggesting that the activation by KOH at 700 °C resulted in a low defect disorder in the internal structure of the material and a high degree of graphitization. Furthermore, HAC-K-700 exhibited relatively prominent broad peaks at the 2D to D + G positions, suggesting the presence of numerous graphite layers in the material. This enhanced its electrical conductivity, thereby improving its electrochemical performance (Zhu et al., 2022).

3.2.3. Isotherm analysis of N_2 adsorption/desorption and pore-size distribution

Figs. 3(a) and 3(b) show the N_2 adsorption–desorption isotherms of the samples, and Figs. 3(c) and 3(d) illustrate the pore-size distribution. HAC-P-700 exhibited negligible adsorption capacity (Fig. 3(a)). For HAC-K-700, the N_2 adsorption rapidly increased with an increase in relative pressure when P/P_0 was below 0.1, indicating the presence of numerous microporous structures. As P/P_0 increased from 0.4 to 0.9, a type-H4 hysteresis loop was observed, suggesting the existence of mesopores induced by capillary condensation. As P/P_0 approached 1.0, the curve exhibited an "upward" tail, indicating the presence of macroporous structures in the material (Huang, Liu, et al., 2016). Fig. 3(b) shows that the micropores in the material gradually decreased with an increase in the activation temperature. The mesoporous fraction of HAC-K-900 was significantly higher than that of other materials, probably attributable to the intense activation of KOH on HA at a high temperature. During the reaction process, some of the microporous structures collapsed, resulting in an excessive formation of mesopores. This led to a reduction in the internal adsorption sites in the material, thereby impeding the diffusion and migration of electrolyte ions in the material (Lv et al., 2012)

Figs. 3(c) and 3(d) show that the micropores of the HAC material were predominantly within the range of 0.4–2 nm; the micropores can provide charge storage sites. However, the mesopores were primarily within the range of 2–6 nm, functioning as ion transport channels. Fig. 3(d) shows that the micropore distribution in the material gradually decreased with an increase in the activation temperature. HAC-K-700 exhibited the highest micropore distribution. Conversely, HAC-K-900 exhibited the highest mesopore distribution, which was consistent with the analysis result of the N_2 adsorption–desorption isotherms. The hierarchical pore structure of HAC-K-700 provided numerous pathways for the rapid transport and diffusion of internal electrolyte ions, thereby enhancing the electrochemical performance of the material.

Differences in the specific surface area can affect battery performance, including capacity, impedance, and charging and discharging rates. Table 2 compares the specific surface areas of electrode materials from different sources. The sludge HAC exhibited the largest specific surface area (1480.53 $m^2 \cdot g^{-1}$). The findings indicated that the sludge HAC had a high potential as an electrode material.

Microporous structures offer relatively large surface areas and active sites, enhancing the reaction rate and catalytic efficiency of electrodes. Mesoporous structures provide improved ion transport pathways, enhancing the diffusion performance and reaction efficiency of electrodes. The appropriate amount of macropores increases the permeability of the electrolyte and electronic transport pathways, thereby improving the permeability and conductivity of electrodes (Shulga et al., 2017). Table 3 shows HAC-K-900 exhibited the highest total pore and mesopore volumes at 1.361 and 1.126 $cm^3 \cdot g^{-1}$, respectively. However, an excessive number of mesopores may cause a decrease in the mechanical strength of the electrode material and the active surface area. HAC-K-700 exhibited the most suitable specific surface area, total pore volume, micropore volume, and mesopore volume (1480.53 $m^2 \cdot g^{-1}$, 0.943 $cm^3 \cdot g^{-1}$, 0.569 $cm^3 \cdot g^{-1}$, and 0.374 $cm^3 \cdot g^{-1}$, respectively). This showed that the KOH activation at 700 °C effectively increased the porous structure of the HAC material and enlarged its specific surface area. The large specific surface area and well-developed pore structure improved charge transfer, thereby enhancing the electrochemical performance.

3.3. Electrochemical characterization

Figs. 4(a) and 4(b) show the CV curves of the materials obtained at a scanning rate of 1 $mV \cdot s^{-1}$. Both curves were rectangular. The good symmetry indicated that the electrode exhibited a high degree of electrochemical reversibility and a stable capacitive process

Table 3
Specific surface area and pore volume data of the materials.

Sample	S_{BET}[a] ($m^2 \cdot g^{-1}$)	V_t[b] ($cm^3 \cdot g^{-1}$)	V_{mic}[c] ($cm^3 \cdot g^{-1}$)	$V_{non\text{-}mic}$[d] ($cm^3 \cdot g^{-1}$)
HAC-P-700	41.67	0.033	0.014	0.019
HAC-Zn-700	584.49	0.329	0.231	0.098
HAC-K-700	1480.53	0.943	0.569	0.374
HAC-K-800	1337.15	0.724	0.504	0.220
HAC-K-900	1257.11	1.361	0.235	1.126

[a] The specific surface area was determined using the BET method.
[b] The total pore volume was measured at a relative pressure of $P/P_0 = 0.98$.
[c] The micropore volume was calculated using the t-plot method.
[d] Vnon-mic represents the difference between the total pore volume and the micropore volume.

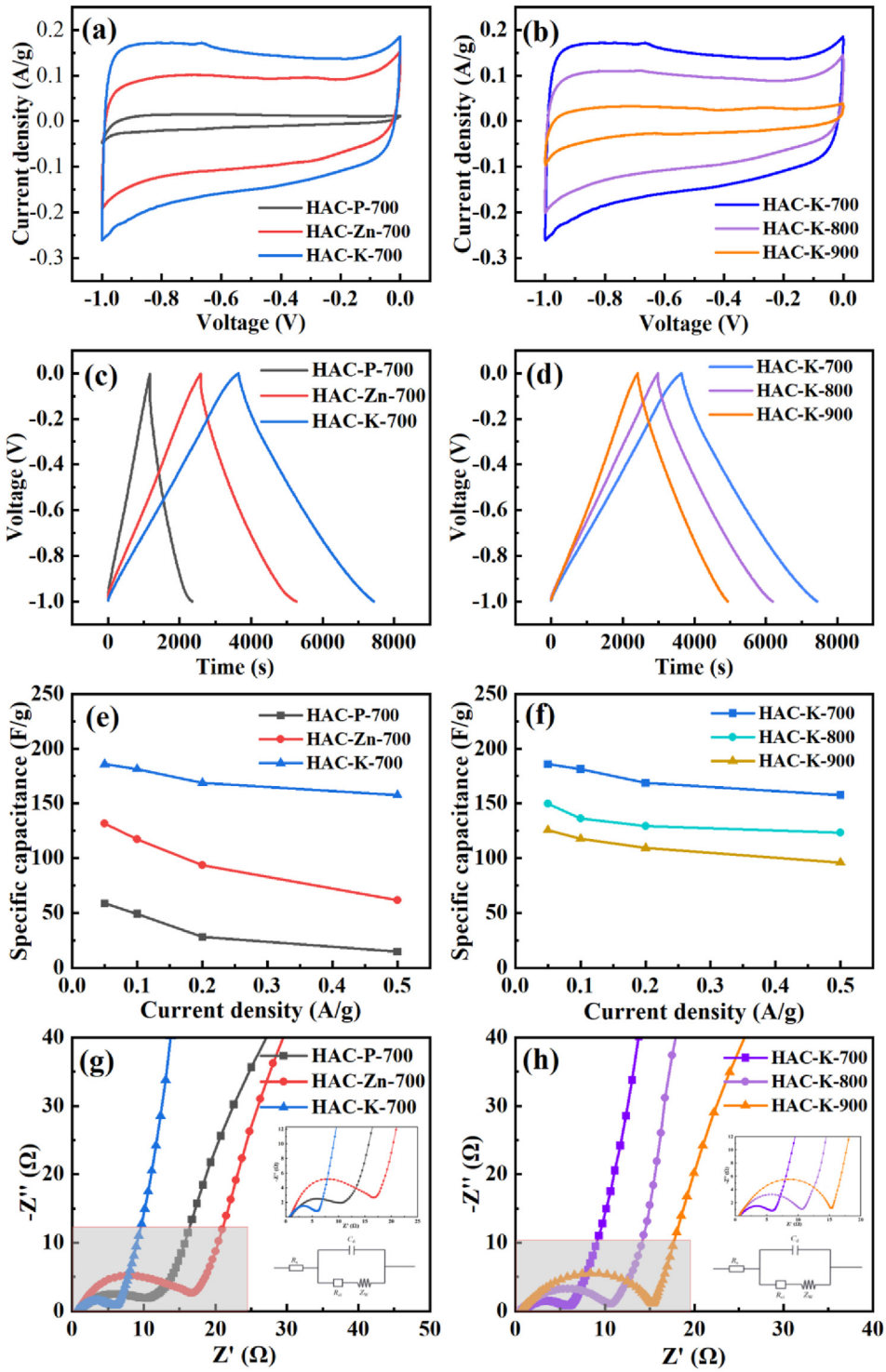

Fig. 4. (a, b) Cyclic voltammetry (CV) curves of the materials at a scanning rate of 1 mV·s^{-1}, (c, d) constant current charge–discharge curves of the materials at a current density of 0.05 A·g^{-1}, (e, f) Specific capacitances of the materials at different current densities, and (g, h) Electrochemical impedance (EIS) curves of the materials.

(Khanh Nguyen et al., 2021). The CV curve of HAC-K-700 exhibited the largest integrated rectangular area, corresponding to a high specific capacitance, suggesting that KOH was highly effective in activating HA at 700 °C.

Figs. 4(c) and 4(d) show the GCD curves of the materials at a current density of 0.05 A·g^{-1}. The isosceles triangular shape indicates the excellent reversibility of the charge and discharge processes in the capacitors, along with a high current efficiency and typical double-layer capacitor characteristics (AlHumaidan et al., 2022). Fig. 4(d) shows that the KOH activation at 700 °C resulted in the longest charge and discharge duration, corresponding to a high specific capacitance. The superior electrochemical performance of HAC-K-700 was primarily attributed to the presence of a graphite-like structure in the material, forming an excellent

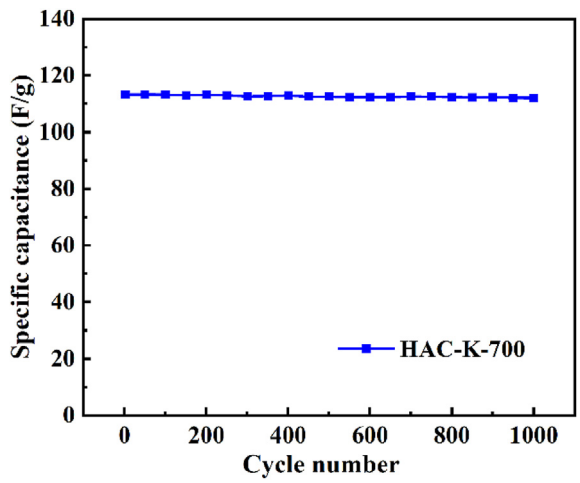

Fig. 5. Cycling stability performance of materials at a current density of 1 $A \cdot g^{-1}$.

conductive network. This reduced the internal resistance of the system, thereby decreasing the voltage drop and enhancing the capacity within the high voltage range.

The line graphs in Fig. 4(e) show the variation in the specific capacitance with the current density for three materials. Comparing the trends and numerical values of the lines, the performance of HAC-K-700 was observed to be superior. At the current densities of 0.05 and 0.5 $A \cdot g^{-1}$, the specific capacitance of HAC-K-700 was 185.9 and 162.1 $F \cdot g^{-1}$, respectively, with a specific capacitance retention rate of 87.2%. The excellent specific capacitance and retention rate reflected the outstanding energy storage and rate performance of the material. Similarly, Fig. 4(f) shows that KOH exhibited superior electrochemical performance at 700 °C, which was consistent with the results of the GCD curves.

Figs. 4(g) and 4(h) show the EIS Nyquist plots of three materials. The radius of the semicircular arc in the high-frequency region was related to the charge-transfer resistance (Coros et al., 2020). The magnitude of the slope of the straight line in the low-frequency region corresponded to the Warburg impedance ($Z\omega$) associated with the migration of electrolyte ions, directly reflecting the diffusion resistance of the electrolyte ions in the materials (Qiao et al., 2021) Figs. 4(g) and 4(h) show that HAC-K-700 exhibited the smallest semicircular arc, indicating a low charge-transfer resistance. This was attributed to the KOH etching process that generated numerous porous structures in the material, resulting in additional active sites to react with oxygen-containing functional groups and promoting internal charge transfer, thereby enhancing the conductivity of the material. Moreover, HAC-K-700 exhibited a higher slope in the low-frequency region than the other materials, indicating the lowest diffusion resistance and providing ion diffusion pathways. This facilitated the rapid internal diffusion of electrolyte ions and improved the capacitance of the material.

HAC-K-700 was subjected to a GCD cycling test at a current density of 1 $A \cdot g^{-1}$ for 1000 cycles to evaluate its cycling stability. The material did not exhibit significant capacity decay after 1000 cycles and retained 97.8% of its initial specific capacitance (Fig. 5). The excellent capacitance indicated that the HAC material obtained through KOH activation at 700 °C exhibited remarkable cyclic stability.

4. Conclusions

(1) Electrode materials prepared from sludge-derived HA hold promise as energy-storage materials because of their cost-effectiveness and favorable electrochemical performance. This may effectively protect the ecological environment and promote the development of green energy sources.

(2) Different activation agents resulted in significant variations in the structural properties of the materials, leading to varying energy-storage performances. Among them, KOH was confirmed to be the most effective activator. HAC-K-700 exhibited a high specific surface area of 1480.53 $m^2 \cdot g^{-1}$ and a rich micro-mesoporous structure. They facilitated the rapid transmission and diffusion of electrolyte ions within the channels, enhancing charge transfer and improving the electrochemical performance of the material.

(3) The activation temperature significantly impacted the pore structure and graphitization degree of the material, with the optimal results obtained at 700 °C. The activation effect of KOH on HA intensified with an increase in temperature. Excessive etching led to the collapse of the internal carbon framework, reduction in the pore structure, and decline in the electrochemical performance of the material.

Declaration of competing interest

The authors state that they do not have any recognizable conflicting financial interests or personal connections that may have seemed to affect the research presented in this paper.

Acknowledgments

The study was financially supported by the Natural Science Research of Shanxi (20210302123071) and the National Key Research and Development Project (2018YFC1801104, 2018YFC-1801105).

References

AlHumaidan, F. S., Rana, M. S., Vinoba, M., Rajasekaran, N., AlHenyyan, H. Y., & Ali, A. A. (2022). Synthesizing few-layer carbon materials from asphaltene by thermal treatment. *Diamond and Related Materials, 129*, 109316.

Cheng, D., Wang, Z., Chen, C., & Zhou, K. (2019). Defect-enriched, nitrogen-doped graphitic carbon microspheres within 3D interconnected super-macropores as efficient oxygen electrocatalysts for breathing Zn-Air battery. *Carbon, 145*, 38–46.

Chen, H., Sun, F., Wang, J., Li, W., Qiao, W., Ling, L., & Long, D. (2013). Nitrogen doping effects on the physical and chemical properties of mesoporous carbons. *Journal of Physical Chemistry C, 117*, 8318–8328.

Climent, M., Ferrer, I., del Mar Baeza, M., Artola, A., Vázquez, F., & Font, X. (2007). Effects of thermal and mechanical pretreatments of secondary sludge on biogas production under thermophilic conditions. *Chemical Engineering Journal, 133*, 335–342.

Coros, M., Varodi, C., Pogacean, F., Gal, E., & Pruneanu, S. M. (2020). Nitrogen-doped graphene: The influence of doping level on the charge-transfer resistance and apparent heterogeneous electron transfer rate. *Sensors, 20*, 1815.

Dai, X. H., Zhang, C., Zhang, L. W., Zhang, R. B., Chen, G., & Hu, W. J. (2021). Thoughts on the development direction of sludge treatment and resource recovery under the background of carbon neutrality. *Water & Wastewater Engineering, 57*(3), 1–5 (in Chinese).

Huang, G., Kang, W., Xing, B., Chen, L., & Zhang, C. (2016). Oxygen-rich and hierarchical porous carbons prepared from coal based humic acid for supercapacitor electrodes. *Fuel Processing Technology, 142*, 1–5.

Huang, G., Liu, Q., Kang, W., Xing, B., Chen, L., & Zhang, C. (2016). Potassium humate based reduced graphite oxide materials for supercapacitor applications. *Electrochimica Acta, 196*, 450–456.

Jia, X. T., Li, Y., Zhang, X. N., Li, X. F., Guo, M. Q., & Yang, L. X. (2022). Research on utilization of sludge through preparation of humic acid-based energy storage materials. *Modern Chemical Industry, 42*(12), 108–113 (in Chinese).

Jiang, L., Cheng, Q., Xia, Y., Pavlinek, V., Saha, P., & Li, C. (2014). Effect of phenolic resin infiltration content on the structural and electrochemical properties of hierarchical porous carbons. *Journal of Materials Science, 49*, 7489–7496.

Khanh Nguyen, V., Kumar Chaudhary, D., Hari Dahal, R., Hoang Trinh, N., Kim, J., Chang, S. W., Hong, Y., La, D. D., Nguyen, X. C., Hao Ngo, H., & Chung, W. J. (2021). Review on pretreatment techniques to improve anaerobic digestion of sewage sludge. *Fuel, 285*, 119105.

Li, L. (2013). Application status and trend on anaerobic digestion technology development of sludge. *China Environmental Protection Industry*, (8), 57–60 (in Chinese).

Li, Y., Jia, X., Li, X., Liu, P., Zhang, X., & Guo, M. (2023). Study on the potential of sludge-derived humic acid as energy storage material. *Waste Management, 162*, 55–62.

Liu, D., Lan, G., Hu, S., & Wang, H. (1992). X-ray diffraction and Raman scattering studies of $HClO_4$-graphite intercalation compounds. *Carbon, 30*, 251–254.

Li, L., Wang, X., Wang, S., Cao, Z., Wu, Z., Wang, H., Gao, Y., & Liu, J. (2016). Activated carbon prepared from lignite as supercapacitor electrode materials. *Electroanalysis, 28*, 243–248.

Li, D., Wang, Q., Yao, Y., Wu, F., Yu, Y., & Zhang, C. (2018). New application of waste citrus maxima peel-derived carbon as an oxygen electrode material for lithium oxygen batteries. *ACS Applied Materials & Interfaces, 10*, 32058–32066.

Lv, Y., Gan, L., Liu, M., Xiong, W., Xu, Z., Zhu, D., & Wright, D. S. (2012). A self-template synthesis of hierarchical porous carbon foams based on banana peel for supercapacitor electrodes. *Journal of Power Sources, 209*, 152–157.

Qiao, Y., Zhang, C., Kong, F., Zhao, Q., Kong, A., & Shan, Y. (2021). Activated biochar derived from peanut shells as the electrode materials with excellent performance in Zinc-air battery and supercapacitance. *Waste Management, 125*, 257–267.

Shulga, Y. M., Baskakov, S. A., Baskakova, Y. V., Lobach, A. S., Volfkovich, Y. M., Sosenkin, V. E., Shulga, N. Y., Parkhomenko, Y. N., Michtchenko, A., & Kumar, Y. (2017). Hybrid porous carbon materials derived from composite of humic acid and graphene oxide. *Microporous and Mesoporous Materials, 245*, 24–30.

Siemieniewska, T., Tomkow, K., Kaczmarczyk, J., Albiniak, A., Grillet, Y., & François, M. (1991). Evaluation of microporosity in steam activated brown coal humic acids chars. In F. Rodriguez-Reinoso, J. Rouquerol, K. S. W. Sing, & K. K. Unger (Eds.), *Studies in surface science and catalysis*. Amsterdam: Elsevier.

Tsutsuki, K., & Kuwatsuka, S. (1978). Chemical studies on soil humic acids. *Soil Science & Plant Nutrition, 24*, 547–560.

Wei, Y. C., Zhou, J., Yang, L., Gu, J., Chen, Z. P., & He, X. J. (2022). N/S co-doped interconnected porous carbon nanosheets as high-performance supercapacitor electrode materials. *New Carbon Materials, 37*, 707–715.

Xing, B., Yuan, R., Zhang, C., Huang, G., Guo, H., Chen, Z., Chen, L., Yi, G., Zhang, Y., & Yu, J. (2017). Facile synthesis of graphene nanosheets from humic acid for supercapacitors. *Fuel Processing Technology, 165*, 112–122.

Yin, J., Zhang, D., Zhao, J., Wang, X., Zhu, H., & Wang, C. (2014). Meso- and microporous composite carbons derived from humic acid for supercapacitors. *Electrochimica Acta, 136*, 504–512.

Yu, K., Wang, Y., Wang, X., Liu, W., Liang, J., & Liang, C. (2019). Preparation of porous carbon anode materials for lithium-ion battery from rice husk. *Materials Letters, 253*, 405–408.

Zhang, M. (2017). Preparation of biomass-derived activated carbon with heteroatom-doped and study of their supercapacitors and oxygen reduction reaction. In *Master's thesis*. China: Beijing University of Chemical Technology.

Zhang, J., Lü, F., Zhang, H., Shao, L., Chen, D., & He, P. (2015). Multiscale visualization of the structural and characteristic changes of sewage sludge biochar oriented towards potential agronomic and environmental implication. *Scientific Reports, 5*, 9406.

Zhao, Y., Huang, S., Xia, M., Rehman, S., Mu, S., Kou, Z., Zhang, Z., Chen, Z., Gao, F., & Hou, Y. (2016). N-P-O co-doped high performance 3D graphene prepared through red phosphorous-assisted "cutting-thin" technique: A universal synthesis and multifunctional applications. *Nano Energy, 28*, 346–355.

Zhu, H., Yin, J., Zhao, X., Wang, C., & Yang, X. (2015). Humic acid as promising organic anodes for lithium/sodium ion batteries. *Chemical Communications, 51*, 14708–14711.

Zhu, J., Zhang, Q., guo, L., Zhao, Y., Zhang, R., Liu, L., & Yu, J. (2022). Highly flexible, freestanding supercapacitor electrodes based on hollow hierarchical porous carbon nanofibers bridged by carbon nanotubes. *Chemical Engineering Journal, 434*, 134662.